32

High-temperature oxidation of $Ti_3Al_{0.7}Si_{0.3}C_2$ in air at 900 °C and 1000 °C*

D. B. Lee and Thuan Dinh Nguyen

Centre for Advanced Plasma Surface Technology, Sungkyunkwan University, Suwon 440-746, South Korea

dlee@yurim.skku.ac.kr

S. W. Park

Multifunctional Ceramic Research Centre, KIST, Seoul 136-791, South Korea

32.1 Introduction

The nanolaminated ternary compound, Ti_3SiC_2, consists of Ti_3C_2 octahedrons stacked along the c-axis which are separated by layers of Si atoms. This compound has been extensively studied for a number of applications, due to its unique combination of both metallic and ceramic properties [1]. It is electrically and thermally conductive, easily machinable, ductile with a high stiffness-to-hardness ratio, thermally stable up to at least 1700 °C in an inert atmosphere, damage tolerant, maintains its strength at high temperatures, and is resistant to thermal shock and chemical attack including high-temperature oxidation. The scales formed on Ti_3SiC_2 are typically composed of an outer TiO_2 layer and an inner (TiO_2+SiO_2) mixed layer [2–4]. Ti_3SiC_2 displays good oxidation resistance because of the presence of SiO_2.

Ti_3AlC_2 is another nanolaminated ternary compound that also exhibits superior metallic and ceramic properties [5]. However, it has been less well studied, owing to the fact that it is a relatively new member of the ternary carbides and because of the difficulties involved in preparing high purity, fully dense specimens [1]. The machinable, layered Ti_3AlC_2 is isostructural with Ti_3SiC_2. Depending on the investigators, inconsistent oxidation resistance and scale morphologies have been reported. For example, Wang and Zhou reported that Ti_3AlC_2 had better oxidation resistance than Ti_3SiC_2, because an adherent, continuous inner Al_2O_3 layer formed below the outer TiO_2 layer [6,7]. In contrast, Barsoum reported that Ti_3AlC_2 had much poorer oxidation resistance than Ti_3SiC_2 because the scales that formed were highly striated, consisting of three repeating layers: an Al_2O_3 layer; a $(Ti_{1-y}Al_y^{\square})O_{2-y/2}$ layer where $y<0.05$; and a porous layer [8,9].

Ti_3SiC_2 and Ti_3AlC_2 form a complete range of solid solutions. Recently, Zhou and colleagues synthesised a $Ti_3Al_{1-x}Si_xC_2$ ($x=0.05\sim0.25$) solid solution using the solid–liquid reaction synthesis and simultaneous densification processes [10,11]. A

* Reprinted from D. B. Lee and T. D. Nguyen: High-temperature oxidation of Ti3Al0.7Si0.3C2 compound at 900 and 1000 °C in air. *Materials and Corrosion*. 2008. Volume 59. pp. 624–8.

mixture of Ti, Al, Si and graphite was used as the starting powder. The synthesis temperature used was 1500 °C, with a soaking time of 1 h, and the hot pressing pressure was 38 MPa of Ar. The $Ti_3Al_{0.75}Si_{0.25}C_2$ that was synthesised displayed excellent oxidation resistance up to 1200 °C for at least 20 h, due to the formation of a continuous α-Al_2O_3 layer, which formed below a thin, discontinuous TiO_2 layer. Silicon existed not only in the TiO_2 layer, but also in the α-Al_2O_3 layer, as $Al_2(SiO_4)O$. A small amount of Ti_5Si_3 precipitated from the $Ti_3Al_{0.75}Si_{0.25}C_2$ solid solution [11].

In the present study, a powder mixture of TiC_X ($x=0.6$), Al and Si was used as the starting powder, and a hot pressing method was used to synthesise highly pure, dense $Ti_3Al_{0.7}Si_{0.3}C_2$ compounds. This new process benefits from simultaneous reaction and densification at a relatively low processing temperature for a short reaction time. Changing the synthesising process and the compound composition would be expected to affect the sample purity, sample density, and the sizes of the matrix grains, which could influence the oxidation kinetics and scale structures significantly. The aim of this study was to describe the high-temperature air-oxidation behaviour of $Ti_3Al_{0.7}Si_{0.3}C_2$ synthesised by the newly developed process. The characteristics of the oxides formed, the distribution and roles of Ti, Al, Si and C in the scale, and the oxidation mechanism are discussed based on the experimental results.

32.2 Experimental

Ti (<45 μm, 99.9% purity) and C (~ 10 μmϕ, 99.95% purity) powders were mixed at a molar ratio of Ti/C = 3:0.67, and pressed at 1500 °C for 3 h under a vacuum of 1.3 Pa. The TiC_X ($x=0.6$) pellets synthesised in this way were ground using a SPEX™ shaker mill, and sieved to a diameter of <45 μm. Powders of TiC_x, Al (<45 μmϕ, 99.9% purity), and Si (<70 μmϕ, 99.9% purity) were mixed at a molar ratio of 3:0.75:0.25 in a SPEX shaker mill for 10 min, and hot pressed at 1400 °C under a pressure of 25 MPa for 60 min in flowing Ar gas. During the hot pressing, a reaction occurred between the TiC_x, Al and Si powders. The synthesised $Ti_3Al_{0.7}Si_{0.3}C_2$ pellets were cut into specimens with dimensions of 10 mm × 5 mm × 5 mm, which were then ground to a 1000 grit finish, ultrasonically cleaned in acetone and methanol, and oxidised isothermally at 900 and 1000 °C in atmospheric air for up to 50 h. The weight changes were continuously monitored as a function of time using a thermogravimetric analyser (TGA). The specimens were investigated by means of a differential thermal analyser (DTA), an Auger electron spectroscope (AES), a scanning electron microscope (SEM) equipped with an energy dispersive spectrometer (EDS), an electron probe micro-analyser (EPMA), and an X-ray diffractometer (XRD) with Cu-Kα radiation.

32.3 Results and discussion

Figure 32.1 shows the SEM microstructure of the synthesised $Ti_3Al_{0.7}Si_{0.3}C_2$. The fully compact specimen has lamellar grains about 10 μm in length and 4 μm in thickness.

Figure 32.2 shows the XRD pattern of $Ti_3Al_{0.7}Si_{0.3}C_2$, along with those of Ti_3AlC_2 and Ti_3SiC_2. These three compounds all have a layered hexagonal structure. Si atoms partially substituted into the Al sites in Ti_3AlC_2 to form $Ti_3Al_{0.7}Si_{0.3}C_2$. Monolithic $Ti_3Al_{0.7}Si_{0.3}C_2$ was successfully synthesised without any impurities. When changing from Ti_3AlC_2 to $Ti_3Al_{0.7}Si_{0.3}C_2$, and then to Ti_3SiC_2, the diffraction angles such as those of the (006), (008), and (104) planes shifted to larger values because the

32.

Relative Intensity

32.

magnitude
a [10].
Figure 3
rate increa
the endoth
reaction, b
Figure
and 1000 °
rutile–TiO
amorphou
small exte
matrix pe

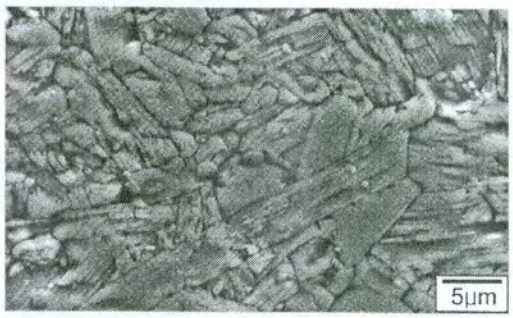

32.1 SEM image of etched $Ti_3Al_{0.7}Si_{0.3}C_2$

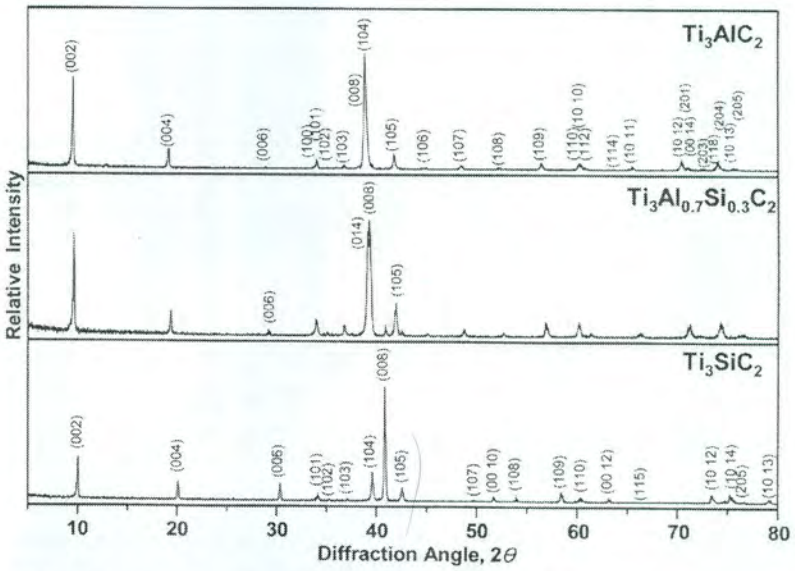

32.2 XRD patterns of $Ti_3Al_{0.7}Si_{0.3}C_2$, Ti_3SiC_2 and Ti_3AlC_2

magnitude of the lattice parameter, *c*, decreased more significantly than that of *a* [10].

Figure 32.3 shows the TG-DTA analytical results for $Ti_3Al_{0.7}Si_{0.3}C_2$. The oxidation rate increased gradually with increasing oxidation temperature. From around 450 °C, the endothermic reaction due to the heating of the sample changed to an exothermic reaction, because $Ti_3Al_{0.7}Si_{0.3}C_2$ began to be oxidised noticeably.

Figure 32.4 shows the XRD patterns of $Ti_3Al_{0.7}Si_{0.3}C_2$ after oxidation at 900 and 1000 °C for 30 h. The oxide scales formed consisted primarily of α-Al_2O_3 and rutile–TiO_2. The SiO_2 that also formed was not detectable using XRD owing to its amorphous structure. The matrix peaks were strong in Fig. 32.4(a), because of the small extent of oxidation. As the oxidation progressed, the scale thickened, and the matrix peaks disappeared. Since the semi-protective TiO_2 grew much faster than

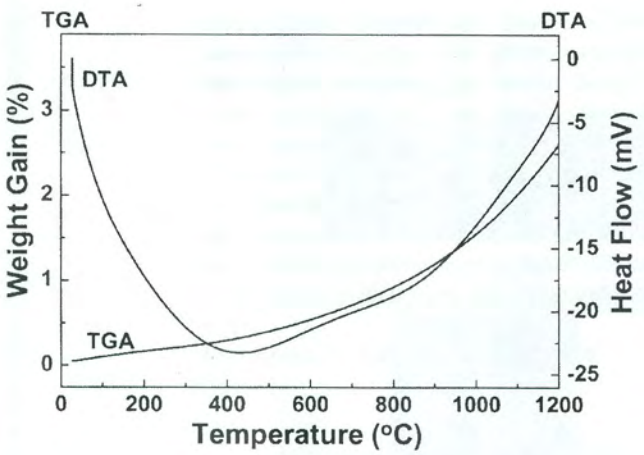

32.3 TG-DTA curves of $Ti_3Al_{0.7}Si_{0.3}C_2$, which were obtained during heating from room temperature to 1200 °C in air with a heating rate of 10 K min ^{1}

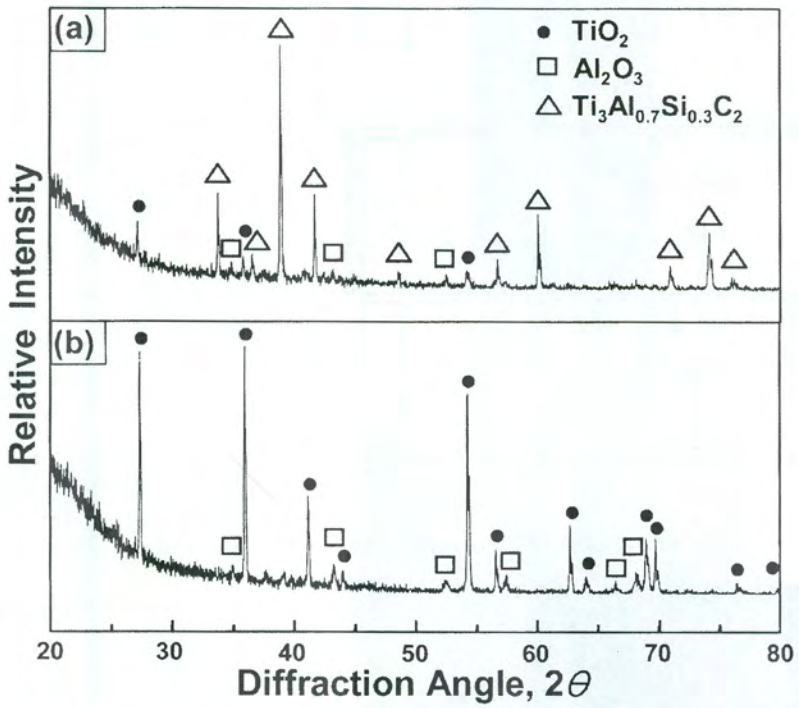

32.4 XRD pattern of $Ti_3Al_{0.7}Si_{0.3}C_2$ after oxidation for 30 h in air: (a) at 900 °C; (b) at 1000 °C

the highly
Fig. 32.4(b
Figure
900 °C for
mechanism
performed
dation. Fr
Ti and Al
Si simply
semicondu
ions or th
defect cor
grow very
stoichiom
known un

Concentration (at.%)

32.
The

the highly protective Al_2O_3, the TiO_2 peaks were stronger than the Al_2O_3 peaks in Fig. 32.4(b). Here, the oxide surface was covered with TiO_2.

Figure 32.5 shows the AES depth profiles of $Ti_3Al_{0.7}Si_{0.3}C_2$ after oxidation at 900 °C for 7 min in air, which were obtained in order to understand the oxidation mechanism during the initial oxidation period. This inert Pt marker experiment was performed by sputter-depositing a thin Pt film on top of $Ti_3Al_{0.7}Si_{0.3}C_2$ before its oxidation. From the location of the Pt film, it is seen that oxygen diffused inwards, while Ti and Al tended to diffuse outwards. Carbon tended to escape from the surface, but Si simply stayed in the $Ti_3Al_{0.7}Si_{0.3}C_2$ sample. It is noted that TiO_2, being an n-type semiconductor, grows primarily by either the outward diffusion of interstitial Ti^{4+} ions or the inward diffusion of O^{2-} ions via oxygen vacancies, depending on the defect concentrations [12]. On the other hand, α-Al_2O_3 is generally known to grow very slowly by the inward diffusion of oxygen [13]. However, the non-stoichiometry in Al_2O_3 is very small, and the defect structure of α-Al_2O_3 is not yet known unequivocally [14].

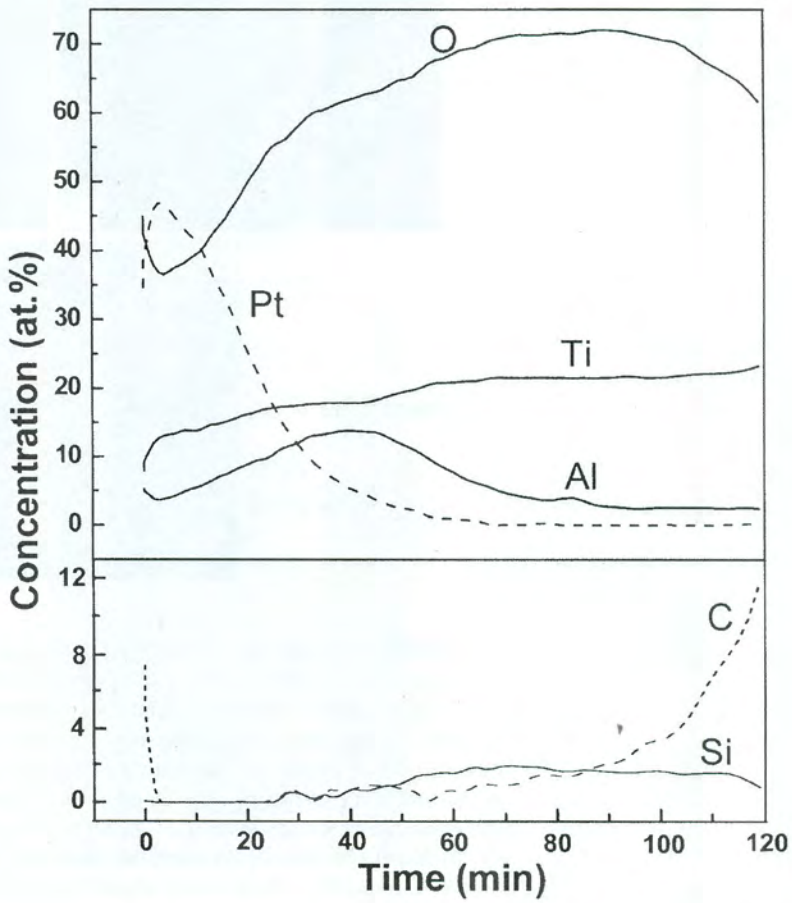

32.5 AES depth profiles of $Ti_3Al_{0.7}Si_{0.3}C_2$ after oxidation at 900 °C for 7 min in air. The penetration rate is 18 nm min^{-1} for reference SiO_2

To understand the oxidation mechanism in the later stages of oxidation, another marker test was performed by spraying fine Pt particles onto the matrix surface before oxidation, as shown in Fig. 32.6. The scale formed after oxidation at 1000 °C for 50 h in air is divided into three layers, namely, an outer TiO_2 layer containing Al_2O_3 particles, an intermediate Al_2O_3 layer, and an inner mixed layer that is rich in TiO_2, but deficient in Al_2O_3 and SiO_2. Platinum particles are located at the top of the intermediate Al_2O_3 layer, indicating that the outer TiO_2 layer grows by the outward diffusion of Ti^{4+} ions, while the inner ($TiO_2 + Al_2O_3 + SiO_2$) mixed layer grows by the inward diffusion of O^{2-} ions. TiO_2 formed by the outward diffusion of Ti^{4+} and the inward diffusion of O^{2-} ions (Fig. 32.6). On the other hand, silicon ions in oxides are relatively immobile, because of the higher bonding energy of Si^{4+}–O^{2-} (465 kJ mol^{-1}). Hence, the Si in the inner mixed layer was oxidised more or less *in situ* by the inwardly diffusing O^{2-} ions. ^{18}O tracer diffusion studies have confirmed that

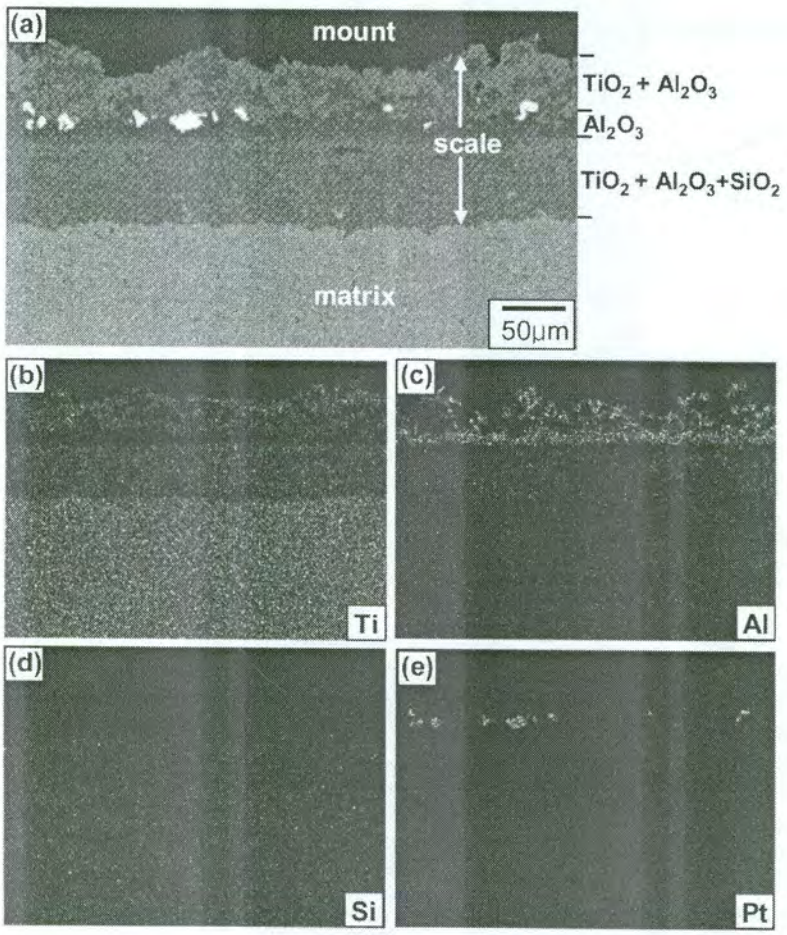

32.6 SEM/EDS analysis on $Ti_3Al_{0.7}Si_{0.3}C_2$ after oxidation at 1000 °C for 50 h in air: (a) cross-sectional back-scattered electron image; (b) Ti map; (c) Al map; (d) Si map; (e) Pt map

the growth of SiO_2 is dominated by inward oxygen diffusion [14]. The Al_2O_3 particles embedded in the outer TiO_2 layer may either be formed by the outward diffusion of Al^{3+} ions (Fig. 32.5), or be the result of the upward migration of Al_2O_3 particles that were originally formed around the intermediate Al_2O_3 layer. The outwardly diffusing Ti^{4+} ions may have induced an upward plastic flow of Al_2O_3 particles. Since the growth rate of TiO_2 is much faster than that of Al_2O_3 and SiO_2 owing to the higher lattice defect concentration, the protectiveness of $Ti_3Al_{0.7}Si_{0.3}C_2$ would depend strongly on the continuity and compactness of the intermediate Al_2O_3 layer. Another barrier to oxidation is the inner mixed layer, containing Al_2O_3 and SiO_2.

Figure 32.7 shows the typical structure of the oxide scale formed on $Ti_3Al_{0.7}Si_{0.3}C_2$. The mature scale consisted of an outer TiO_2 layer containing Al_2O_3 particles, an

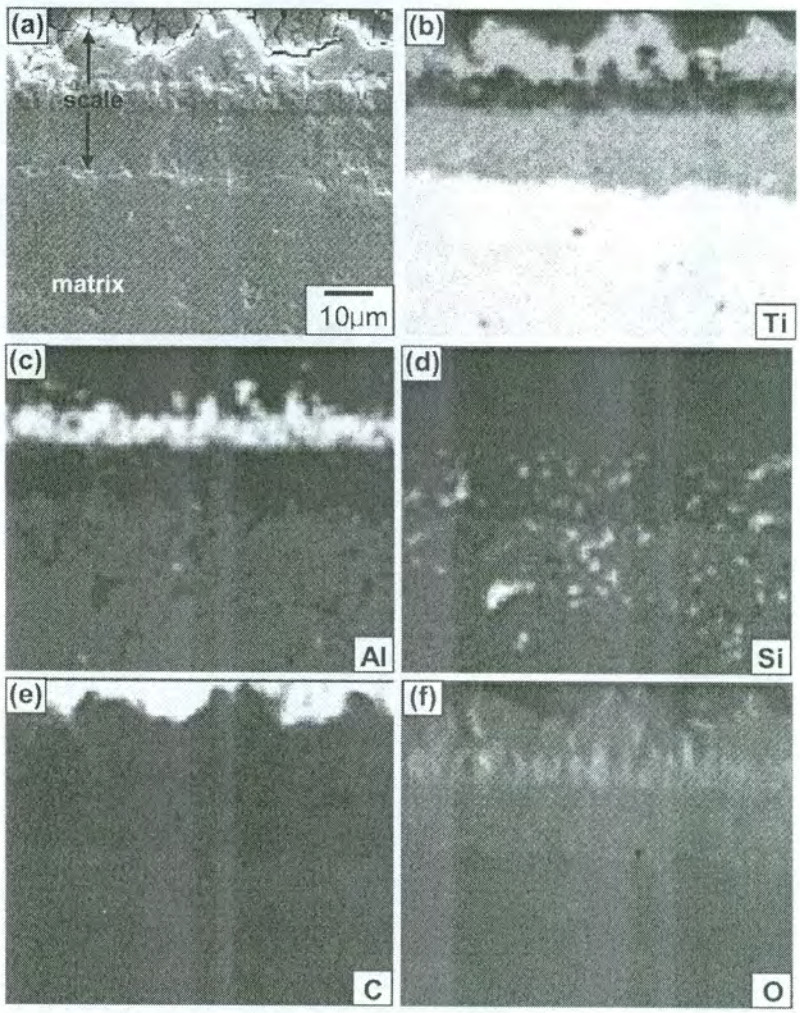

32.7 EPMA analysis of $Ti_3Al_{0.7}Si_{0.3}C_2$ after oxidation at 1000 °C for 30 h in air: (a) cross-sectional image; (b) Ti map; (c) Al map; (d) Si map; (e) carbon map; (f) oxygen map

intermediate Al_2O_3 layer, and a TiO_2-rich, inner mixed oxide layer. Carbon is hardly seen in the scale, owing to its liberation as CO or CO_2 gases. Upon its exposure to oxygen, the surface of $Ti_3Al_{0.7}Si_{0.3}C_2$ would be covered with TiO_2, Al_2O_3, and SiO_2 crystallites, because no equilibrium exists between the gas phase and the matrix. Rutile, having the highest growth rate, soon overgrows alumina and silica and progressively covers the entire surface, forming coarse outer oxide grains. The outwardly moving Ti ions may carry a certain amount of Al ions with them towards the surface, forming Al_2O_3 particles inside the outer TiO_2 layer. The consumption of Ti at the outer surface depletes the Ti immediately below and thereby enriches the Al enough to form an intermediate Al_2O_3 layer. This layer contains interdispersed TiO_2 particles, so that oxygen can diffuse through the intermediate Al_2O_3 layer down to the matrix. Al_2O_3 itself is highly stable, and exhibits low diffusivities for both cations and anions. Since the amount of Si in $Ti_3Al_{0.7}Si_{0.3}C_2$ is small, the SiO_2 that is formed exists as scattered particles in the inner mixed oxide layer. Here, rather strong Al-depletion occurs owing to the consumption of the Al above. Since there is still enough Ti below the intermediate Al_2O_3 layer, the inner mixed oxide layer is rich in TiO_2.

Figure 32.8(a) shows the appearance of the oxide scale formed on $Ti_3Al_{0.7}Si_{0.3}C_2$ that was oxidised at 1000 °C for 5 h in air. Initially formed tiny oxide crystallites were

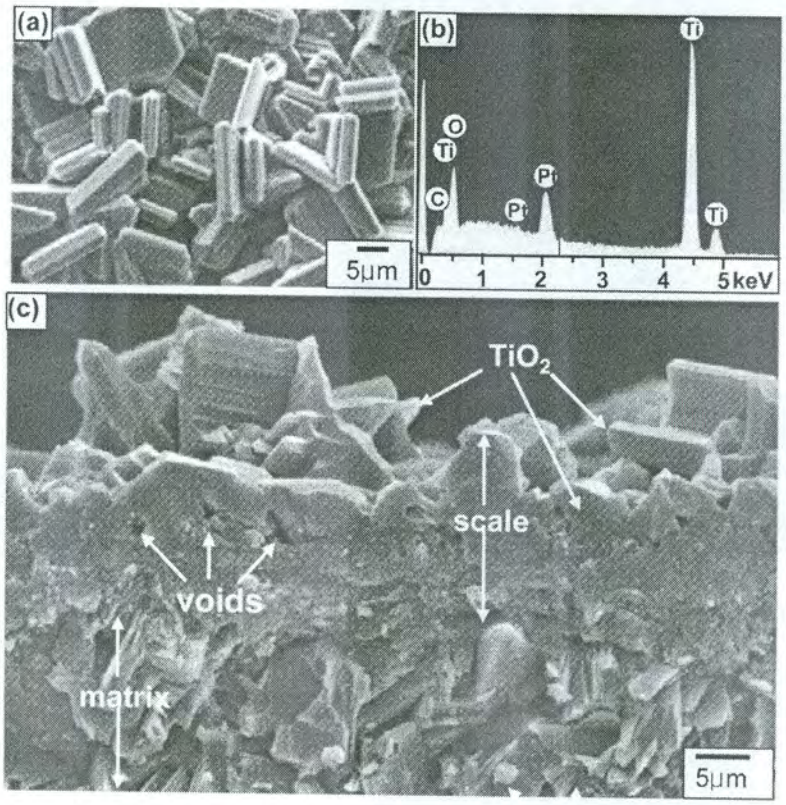

32.8 SEM analysis of $Ti_3Al_{0.7}Si_{0.3}C_2$ after oxidation at 1000 °C for 5 h in air: (a) top view; (b) EDS spectrum of (a); (c) fractograph

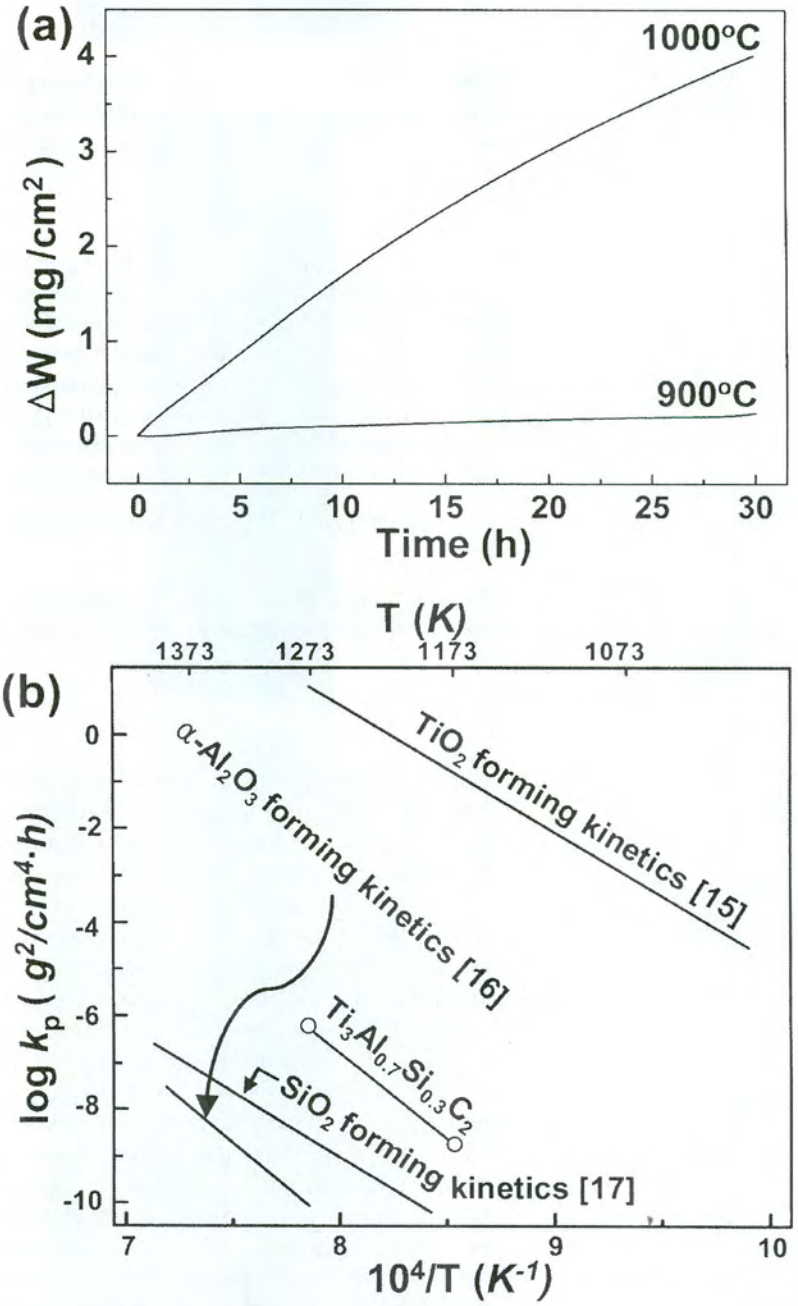

32.9 (a) Isothermal oxidation kinetics of $Ti_3Al_{0.7}Si_{0.3}C_2$ at 900 and 1000 °C in air; (b) temperature dependence of the parabolic rate constants for $Ti_3Al_{0.7}Si_{0.3}C_2$. The k_p values of TiO_2 [15], α-Al_2O_3 [16], and SiO_2 [17] are superimposed

grown into the characteristic pillar-like, coarse rutile–TiO_2. The corresponding EDS spectrum shown in Fig. 32.8(b) indicates that the whole surface was covered with TiO_2. The fractograph shown in Fig. 32.8(c) displays the TiO_2 grains that formed at the outer surface. Partial sintering of the coarse TiO_2 grains is evident. The intermediate Al_2O_3 grains and the inner mixed oxide grains are inevitably fine, because alumina and silica grow quite slowly and suppress the grain growth of the intermixed titania. Microscopic voids are seen at the interface between the outer TiO_2 grains and the intermediate Al_2O_3 grains. Voids form due to the Kirkendall effect caused by the outward diffusion of Ti ions, the escape of carbon in the form of CO or CO_2, and the mismatch in the volume expansion between the TiO_2 and Al_2O_3 grains. Such voids provide the channel for oxygen diffusion and act as stress concentrators and, therefore, adversely affect the scale integrity or adherence. The lamellar $Ti_3Al_{0.7}Si_{0.3}C_2$ grains were disintegrated into fine oxide grains at the oxidation front. This oxidation front is not ideally uniform, owing to the anisotropy of the matrix grains.

Figure 32.9(a) shows the weight gain vs. oxidation time curves of $Ti_3Al_{0.7}Si_{0.3}C_2$ at 900 and 1000 °C. $Ti_3Al_{0.7}Si_{0.3}C_2$ oxidises almost parabolically, indicating that the oxidation process is diffusion controlled. The weight gain increased with increasing oxidation temperature. The scale thicknesses measured after oxidation at 900 and 1000 °C for 30 h were 5 and 42 μm, respectively. The curves shown in Fig. 32.9(a) were fitted to the equation, $\Delta W^2 = k_p \cdot t$, where ΔW is the weight gain per unit area, t is the oxidation time, and k_p is the parabolic rate constant. From Fig. 32.9(b), it is seen that $Ti_3Al_{0.7}Si_{0.3}C_2$ oxidises considerably more slowly than the TiO_2-forming kinetics [15], but faster than the α-Al_2O_3-forming [16] and SiO_2-forming [17] kinetics. The activation energy for the oxidation of $Ti_3Al_{0.7}Si_{0.3}C_2$ obtained from Fig. 32.9(b) was 706.5 (kJ mol^{-1}).

32.4 Conclusions

Fully dense, monolithic $Ti_3Al_{0.7}Si_{0.3}C_2$ compounds having lamellar grains were oxidised in air. $Ti_3Al_{0.7}Si_{0.3}C_2$ oxidised almost parabolically at 900 and 1000 °C according to the equation

$$Ti_3Al_{0.7}Si_{0.3}C_2 + O_2 \rightarrow \text{rutile–}TiO_2 + \alpha\text{-}Al_2O_3 + \text{amorphous } SiO_2 + (CO \text{ or } CO_2)$$

The oxidation proceeded primarily by the simultaneous inward diffusion of oxygen ions to form an inner mixed oxide layer that was rich in TiO_2, but deficient in Al_2O_3 and SiO_2, and the outward diffusion of Ti ions to form an outer TiO_2 layer. These oxide layers were separated by an intermediate Al_2O_3 layer. The silicon in the inner mixed oxide layer was less mobile, and was oxidised more or less *in situ* by the inwardly diffusing oxygen ions. The Al_2O_3 particles embedded in the outer TiO_2 layer may be formed by either the outward diffusion of Al^{3+} ions or the upward plastic flow of Al_2O_3 particles owing to the outwardly diffusing Ti^{4+} ions.

Acknowledgments

This work was supported by a grant (no. R-11-2000-086-0000-0) from the Center of Excellency Program of the KOSEF, and by a grant (no. 05K1501-00610) from the 'Center for Nano-Structured Materials Technology' under the 21st century frontier R&D programme of the MOST, Korea.

Referenc

1. M. W.
2. M. W. 2508.
3. M. W. (2003).
4. Z. Sun,
5. N. V. T
6. X. H. V
7. X. H. V
8. M. W.
9. M. W.
10. Y. C. Z
11. J. X. C
12. Y. M. (Sons, N
13. R. Pres
14. P. Kofs
15. P. Kofs
16. M. W.
17. I. C. I.

References

1. M. W. Barsoum, *Prog. Solid State Chem.*, 28 (2000), 201.
2. M. W. Barsoum, T. El-Raghy and L. U. J. T. Ogbuji, *J. Electrochem. Soc.*, 144 (1997), 2508.
3. M. W. Barsoum, L. H. Ho-Duc, M. Radovic and T. El-Raghy, *J. Electrochem. Soc.*, 150 (2003), B166.
4. Z. Sun, Y. Zhou and M. Li, *Corros. Sci.*, 43 (2001), 1095.
5. N. V. Tzenov and M. W. Barsoum, *J. Am. Ceram. Soc.*, 83 (2000), 825.
6. X. H. Wang and Y. C. Zhou, *Corros. Sci.*, 45 (2003), 891.
7. X. H. Wang and Y. C. Zhou, *Acta Mater.*, 50 (2002), 3141.
8. M. W. Barsoum, *J. Electrochem. Soc.*, 148 (2001), C551.
9. M. W. Barsoum, *J. Electrochem. Soc.*, 148 (2001), C544.
10. Y. C. Zhou, J. X. Chen and J. Y. Wang, *Acta Mater.*, 54 (2006), 1317.
11. J. X. Chen and Y. C. Zhou, *Oxid. Met.*, 65 (2006), 123.
12. Y. M. Chiang, D. P. Birnie III and W. D. Kingery, *Physical Ceramics*, 109, John Wiley & Sons, NY, 1996.
13. R. Prescott and M. J. Graham, *Oxid. Met.*, 38 (1992), 233.
14. P. Kofstad, *Oxid. Met.*, 44 (1995), 3.
15. P. Kofstad, *High Temperature Oxidation of Metals*, 175, John Wiley & Sons, NY, 1966.
16. M. W. Brumm and H. J. Grabke, *Corros. Sci.*, 33 (1992), 1677.
17. I. C. I. Okafor and R. G. Reddy, *JOM*, 51(6) (1999), 35.